ACS OMEGA

Open Access

http://pubs.acs.org/journal/acsodf

Article

Novel Life Prediction Method of PMMA for Cultural Relics Protection Based on the BP Neural Network

Yang Zhang, Ke Wang, Hao Peng, Xuegang Liu,* Yanfen Huang, Hai An, and Yang Lei*

Cite This: *ACS Omega* 2023, 8, 47812−47820

Read Online

ACCESS | Metrics & More | Article Recommendations | Supporting Information

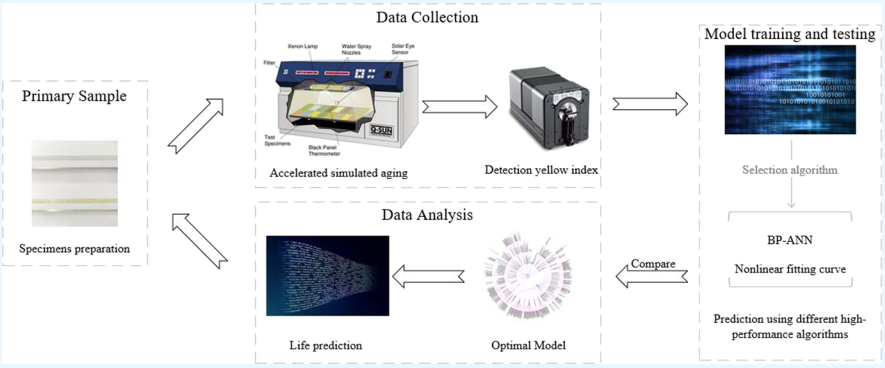

ABSTRACT: Poly(methyl methacrylate) (PMMA) is widely used in the preservation and exhibition of cultural relics in museums. Accurately predicting its service life can help avoid many negative effects caused by PMMA aging. To study the change in the yellowing index of PMMA after aging in a UV light environment, an aging experiment was conducted. A prediction model for the service life of PMMA was established using nonlinear curve fitting and a back propagation (BP) neural network. By comparing the goodness of fit, simulation and modeling capabilities of the initial data, and the predictive ability for new data, it was found that the BP neural network prediction model outperformed the nonlinear curve fitting prediction model. In this study, the service life of newly produced PMMA samples was calculated as 7.83, 8.47, and 8.42 years, based on the yellowing index of retired PMMA as a benchmark and using the output data from the BP neural network prediction model. At this time, the performance and exhibition effect of the PMMA are poor, and the batch of PMMA needs to be updated.

1. INTRODUCTION

Poly(methyl methacrylate) (PMMA) has the advantages of high transparency, high mechanical strength, lightweight, easy processing, good dielectric properties, and insulation, and has been widely used in various fields such as architecture, aviation, medicine, and the chemical industry.[1−6] It is also used in museum artifact preservation and exhibition, allowing archeologists and other researchers to directly observe artifacts. Due to the characteristics of this organic polymer material, long-term exposure to sunlight and air can result in a certain degree of aging, which manifests as molecular chain degradation and molecular weight reduction at the microscopic level, and a decrease in optical properties such as light transmittance, as well as reduced toughness, tensile strength, and fatigue strength at the macroscopic level.[7] Therefore, it is necessary to regularly check its aging degree and replace it according to a cycle to prevent the reduction of light transmittance and yellowing caused by PMMA aging from affecting the display effect of artifacts or even causing them to crack and damage.

The issue of the aging of PMMA has long been a concern, and scholars at home and abroad have conducted many aging tests on this topic. Research has shown that climate and environmental factors, such as sunlight, oxygen, ozone, temperature, and humidity, can cause PMMA to age, with temperature, humidity, and sunlight being the main factors. PMMA exposed to sunlight undergoes photodegradation, where the polymer absorbs radiation, promotes chemical reactions, and changes the material's physical and mechanical properties. The yellowing index test and the degree of yellowing observed in PMMA under sunlight exposure correlate well, so the aging degree of PMMA can be evaluated by testing its yellowing index. In specific environments, studying the degree of aging of PMMA to determine its service life has significant importance. Combining test data with intelligent algorithms is a good method, in which test data are obtained through aging tests, the intelligent algorithm's

Received: August 23, 2023
Revised: November 2, 2023
Accepted: November 28, 2023
Published: December 8, 2023

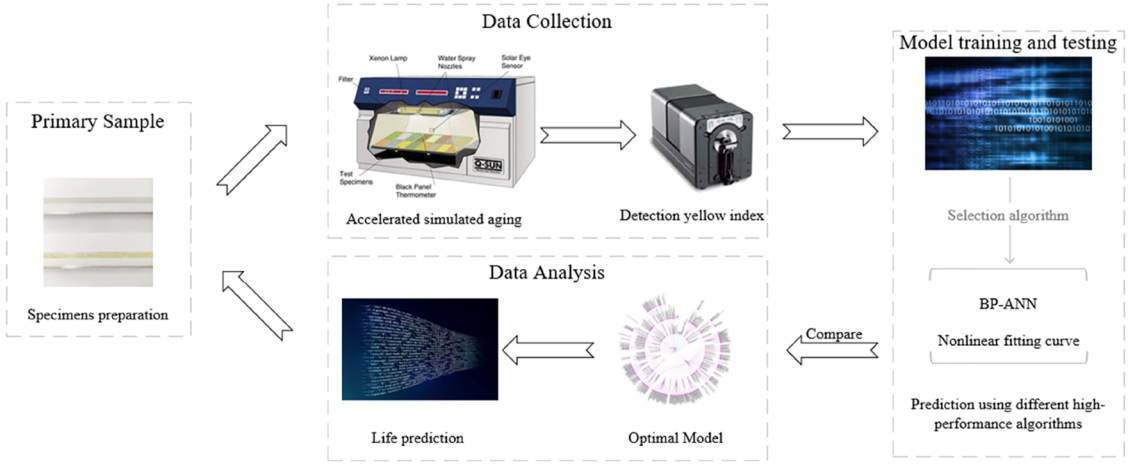

Figure 1. Modeling strategy for life prediction based on the PMMA yellow index.

parameters are continuously adjusted to obtain an accurate model, and the conclusion is obtained through simulation.[8−10] Scholars at home and abroad have made certain theoretical achievements and practical experiences in predicting material life and indicate that neural networks have good performance.[11]

For years, numerous studies have been conducted on the accelerated aging of PMMA and its longevity prediction. In the experimental study of artificially accelerating the aging of PMMA, Yin et al.[12] investigated the aging behavior of PMMA under different temperatures and static tensile forces in liquid scintillators. It was found that an increase in aging temperature led to a rapid decrease in the tensile strength of PMMA, and the time−temperature superposition method was used to predict the service life of PMMA. Murray et al.[13] exposed two types of PMMA to high-intensity UV radiation and focused xenon arc, and pointed out that compared to xenon arc, UV radiation caused a 3−6 times increase in photodegradation of PMMA. Yousif and Haddad[14] reported that photodegradation is the main cause of deterioration in the aging resistance of polymers when exposed to UV radiation. Miller et al.[15] studied the effect of UV light, temperature, and humidity on the aging of PMMA materials using an aging test bench equipped with a xenon lamp and compared the results of outdoor exposure tests to predict the service life of these materials. de Castro Monsores et al.[16] placed PMMA in a UV−B accelerated aging chamber for 811 h and found that UV radiation can change the hardness of PMMA, leading to a decrease in its fracture elongation and tensile strength.

In the neural network prediction study based on the experimental data, Kechagias et al.[17] employed a feedforward and backpropagation neural network (FFBP-NN) to predict the geometry of PMMA thin plates cut by a CO_2 laser. Kuo et al.[18] integrated a backpropagation neural network (BPNN) with the Levenberg−Marquardt (LM) algorithm to establish a prediction system for the CO_2 laser processing of light guide plates. Chen et al.[19] utilized neural networks and multiple linear regression analysis to forecast the glass transition temperature of polymers. Asante-Okyere et al.[20] developed feedforward backpropagation (FFBP) and generalized regression neural network (GRNN) models to predict the flammability of PMMA. Khanlou et al.[21] applied response surface methodology and artificial neural networks (ANNs) to predict and optimize the parameters of the electrospinning process for PMMA nanofibers. Kimmig et al.[22] introduced a method for predicting nanoparticle size, combining multilayer graph convolutional networks with fully connected neural networks. D'Addona et al.[23] utilized ANN computing technology to predict the depth and surface roughness of PMMA laser milling tests. Wiangkham et al.[24] employed an artificial intelligence approach, combining ANN and adaptive neural fuzzy reasoning system (ANFIS), to predict the mixed mode I/II fracture toughness of PMMA materials. Paturi et al.[25] successfully predicted the optimal weld width and indentation depth of PMMA products in the plastic injection molding process using an ANN model. Chen et al.[26] forecasted the water absorption of PMMA and its composite materials using a BP neural network. Sadan et al.[27] employed ANN to quantitatively estimate the membrane diameter of PMMA nanofibers. However, there are few studies on using neural networks for predicting the service life of PMMA. It is possible to establish corresponding models and equations for prediction using the data obtained from accelerated aging tests, based on the principle of consistency between the mechanisms of artificial accelerated aging and the natural aging of PMMA.[28]

In this study, we employ a data-driven machine learning (ML) algorithm to predict the lifetime of PMMA. Obtaining material life data through experiments usually takes a lot of time and resources, and ML models can analyze large-scale data in a relatively short time, thus speeding up the process of predicting material life and reducing the cost of experiments. The use of ML methods can not only predict the life of materials more accurately in complex environments but also help improve the reliability of material design and engineering applications. Therefore, based on the accelerated aging test of PMMA simulated by a xenon lamp, the life prediction model of the yellow index was established by using two ML algorithms of nonlinear curve fitting and BPNN. The degree of initial data fitting, simulation and modeling ability, and new data prediction ability of nonlinear curve fitting and the BPNN prediction model are compared.

2. MODELING STRATEGY

In this work, a novel modeling strategy based on the yellow index is used to predict the life of PMMA, as shown in Figure 1. First, PMMA samples were subjected to a xenon lamp accelerated aging test for 180 days, and the yellow index of different aging times was tested; second, the life prediction

https://doi.org/10.1021/acsomega.3c06140
ACS Omega 2023, 8, 47812−47820

model was established based on the yellow index, and the optimal algorithm is selected by comparing the nonlinear fitting curve with the BPNN. Finally, by calculating the time correspondence between natural aging and accelerated aging, combined with predicted values, it can be used for predicting the lifespan of PMMA.

3. EXPERIMENTAL SECTION

3.1. Specimens Preparation. This experiment used the newly produced PMMA as shown in Figure 2a and the PMMA

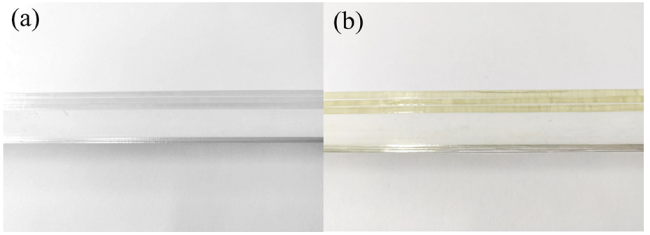

Figure 2. (a) New PMMA. (b) PMMA after eight years of use.

as shown in Figure 2b that has been used for eight years provided by the Jingzhou Cultural Relics Protection Center. The original plate was made into 6 specimens of 30 mm × 20 mm × 4 mm specifications.

3.2. Aging Test. The text describes a testing method for plastics using laboratory light sources, as outlined in GB/T 16422.1-2019 (Plastics—Laboratory Light Sources Exposure Test Method Part 1: General Principles) and GB/T 16422.2-2022 (Plastics—Laboratory Light Sources Exposure Test Method Part 2: Xenon Arc Lamp). To simulate natural exposure environments, a PMMA specimen is placed in a Q-SUN Xe-1 desktop xenon lamp accelerated aging test chamber, with a set blackboard temperature of (50 ± 5 °C), a wavelength of 340 nm, relative humidity of (70 ± 5)%, and an irradiation interval of 1 day, with each irradiation lasting 5 days. The cumulative irradiation time is 180 days, and a yellowing index test is conducted every 15 days by taking specimens.

3.3. Characterization of the Yellow Index of Specimens. According to ASTM E313-2010 (Standard Practice for Calculating Yellowness and Whiteness Indices from Instrumentally Measured Color Coordinates), measurements were taken using a Color i7 spectrophotometer. The three stimulus values X, Y, and Z of the samples were measured under a D65 light source and a 10° standard observer. The yellowing index was then calculated using eq 1

$$\mathrm{YI} = \frac{100(C_X X - C_Z Z)}{Y} \tag{1}$$

3.4. Experimental Results and Discussion. The morphologies of the PMMA before and after xenon lamp accelerated aging are shown in Figure 3, with the old sample on the left and the new sample on the right. As can be seen from the two images, before accelerated aging, the old sample had a yellowish color, while the new sample was relatively transparent. After accelerated aging, the yellowing of the old sample slightly intensified, while the new sample began to show a slight yellowing with a relatively small observable change in color.

The test results are listed in Figure 4. It can be seen that the initial yellow index of the two kinds of PMMA is quite

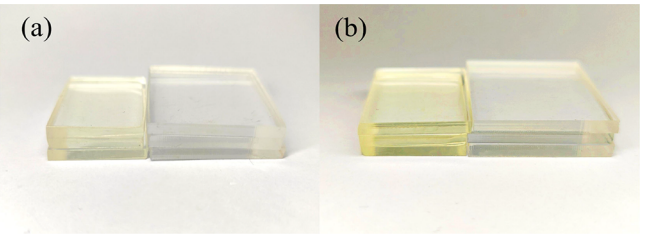

Figure 3. (a) Specimens before and after aging. (b) Specimens after aging.

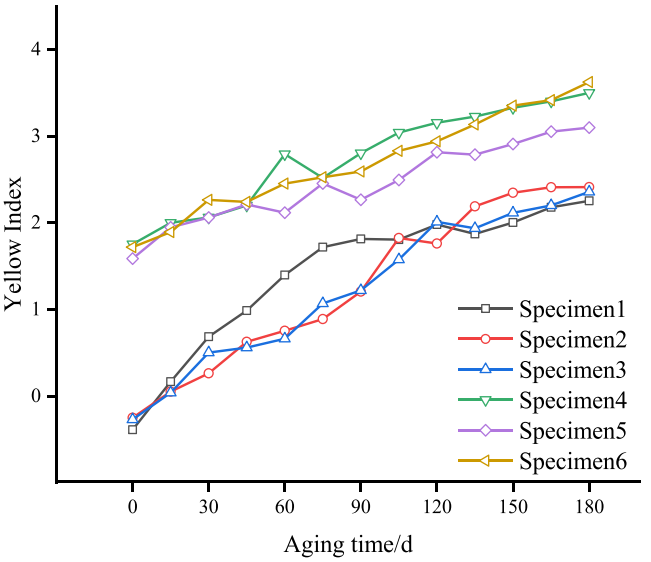

Figure 4. Yellow index at different aging times.

different. The initial yellow index of the new sample of PMMA is about 0.5, while the initial yellow index of the old sample of PMMA is about 2.5. With the increase in aging time, the yellow index of both kinds of PMMA showed an upward trend, and the rising rate of the yellow index of the new sample was significantly higher than that of the old sample. This indicates that the new sample is more susceptible to the aging process, and its yellow color changes faster. In the aging process, the yellow index of new samples increased significantly, while the yellow index of old samples increased slowly. This indicates that the physical and chemical structure of PMMA has changed rapidly in the early stage of the aging process, leading to the rapid increase of the yellow index. However, in the late aging period, the change rate of its physical and chemical structure is relatively slow, leading to the slow increase rate of the yellow index. The test results are shown in Appendix I in the supplementary file.

According to the test data, the average yellow index of natural aging in the museum environment for eight years is about 2.5, which is equivalent to the artificial accelerated aging time of about 105 days. According to the aging time calculation in eq 2, the aging factor B is equal to 681.96.

$$T = \left(\frac{A}{B}\right)^{DT/10} \tag{2}$$

$$B = \frac{A}{T^{10/DT}} \tag{3}$$

https://doi.org/10.1021/acsomega.3c06140
ACS Omega 2023, 8, 47812−47820

where T is the aging time, A is the actual days, B is the aging factor, and DT is the difference between the actual temperature and aging temperature. The aging temperature is 55 °C, and the actual temperature is 23 °C.

4. LIFE PREDICTION

4.1. Nonlinear Fitting Curve. In scientific experiments, the functional relationship between the independent variable x and the dependent variable y sometimes cannot be directly expressed but can only obtain the function value or derivative value of the function at several points.[29] When the value of a function outside the observation point is required, it is necessary to estimate the value of the function at that point. Based on the values of the observation points, construct a relatively simple function $y = \partial(x)$, so that the value of the function at the observation point is equal to the known numerical value or derivative value. To find such a function, $\partial(x)$, based on the accuracy of the measurement data, there are two methods for processing the observation data:

(1) The measured values are accurate and have no errors compared to the true values, and interpolation is generally used;
(2) When there are errors between the measured values and the true values, curve fitting is generally used.

The nonlinear curve fitting algorithm can be customized according to the specific problem, and the appropriate function form and parameters can be selected. This ability to customize allows them to adapt more quickly to the needs of specific problems. In addition, in the case of small amounts of data, nonlinear curve fitting algorithms are usually better adapted to the data and can provide more reliable models. In nonlinear fitting, with experimental data (x_i, y_i), $(i = 1, 2,...,n)$, search for the function $f(x, \hat{y})$ to minimize the sum of squares of the deviation between the function values at points x_i, $(i = 1, 2,...,n)$ and the observed data. Find the functions x and y that meet the following conditions, and find the minimum value of $\sum_{i=1}^{n} (f(x_i, \hat{y}) - y_i)^2$. To solve such problems, the following steps can be taken:

(1) First, make a scatter plot and determine the type of function;
(2) Determine the initial value of the unknown parameters based on the known data, and calculate the best parameters;
(3) Compare the fitting effect based on the coefficient of determination.

The accuracy of the prediction performance is evaluated by the determination coefficient R^2 (Goodness of fit). The larger the determination coefficient, the better the Goodness of fit. Let y be the value to be fitted, with an average value of $\bar{y}$ and a fitted value of $\hat{y}$.

$$\mathrm{SST} = \sum_{i=1}^{n} (y_i - \bar{y})^2 \tag{4}$$

$$\mathrm{SSR} = \sum_{i=1}^{n} (\hat{y}_i - \bar{y})^2 \tag{5}$$

$$\mathrm{SSE} = \sum_{i=1}^{n} (y_i - \hat{y}_i)^2 \tag{6}$$

$$R^2 = \frac{\mathrm{SSR}}{\mathrm{SST}} = \frac{\sum_{i=1}^{n} (\hat{y}_i - \bar{y})^2}{\sum_{i=1}^{n} (y_i - \bar{y})^2} = 1 - \frac{\mathrm{SSE}}{\mathrm{SST}} \tag{7}$$

Table 1. Yellowing Index of PMMA at Different Aging Times

aging time/day	yellowing index		
	specimen 1	specimen 2	specimen 3
0	0.4672	0.6028	0.5813
15	1.0181	0.9028	0.8927
30	1.5343	1.1224	1.3502
45	1.8414	1.4509	1.4078
60	2.2382	1.6017	1.5120
75	2.5385	1.7377	1.9244
90	2.6613	2.0411	2.0632
105	2.6335	2.6739	2.4406
120	2.8126	2.6202	2.8463
135	2.7130	3.0304	2.7927
150	2.8608	3.1952	2.9534
165	3.0179	3.2120	3.0430
180	3.0984	3.2524	3.1840

4.1.1. Variable Selection. The yellowing index from 0 to 180 days in the xenon lamp accelerated aging test of PMMA was selected as shown in Table 1 for variable selection. The output variable for the model is the yellowing index Y, and the input variable is the aging time X.

4.1.2. Model Construction. The allometric function was used and nonlinear least-squares based on the Levenberg–Marquardt algorithm (LMA) were employed for model construction.[30] The maximum number of iterations was set to 100, and the error tolerance was set to 10^{-9}. The fitting equation $y = ax^b$ was used to simultaneously fit specimens 1, 2, and 3.

4.1.3. Model Validation. The fitted curve output is $y = 0.23377x^{0.50761}$, with a standard error of 0.03332 for the a value and 0.02991 for the b value. The fitting results are listed in Figure 5. From the perspective of fitting goodness, the sum of squared residuals is 1.44598, the mean squared error (MSE) is 0.03908, R^2 is 0.92635, and the adjusted R^2 is 0.92419, which is close to 1. This indicates that the equation has a high degree of fitting goodness and that the independent variable can accurately explain the variability in the dependent variable with an accuracy rate of over 92.4%.

4.2. Back Propagation Neural Network. ANN is a model for parallel distributed information processing that imitates the structure of human brain neurons and neural networks. It does not require a predetermined mathematical equation to map the relationship between input and output but instead learns a certain rule through its training to produce results closest to the expected output given a specific input value. There are many models of ANNs, but the most widely used and intuitive is the multilayer feedforward neural network with an error backpropagation learning algorithm. The BPNN was proposed in 1986 by a group of scientists led by Rumelhart and McClelland. It is a powerful nonlinear model that can adapt to various complex nonlinear relationships, which makes it more flexible in dealing with practical problems. The multilayer structure of the BPNN allows hierarchical feature learning. By abstracting the features of data layer by layer, the network can learn the representation of multiple levels in the

https://doi.org/10.1021/acsomega.3c06140
ACS Omega 2023, 8, 47812−47820

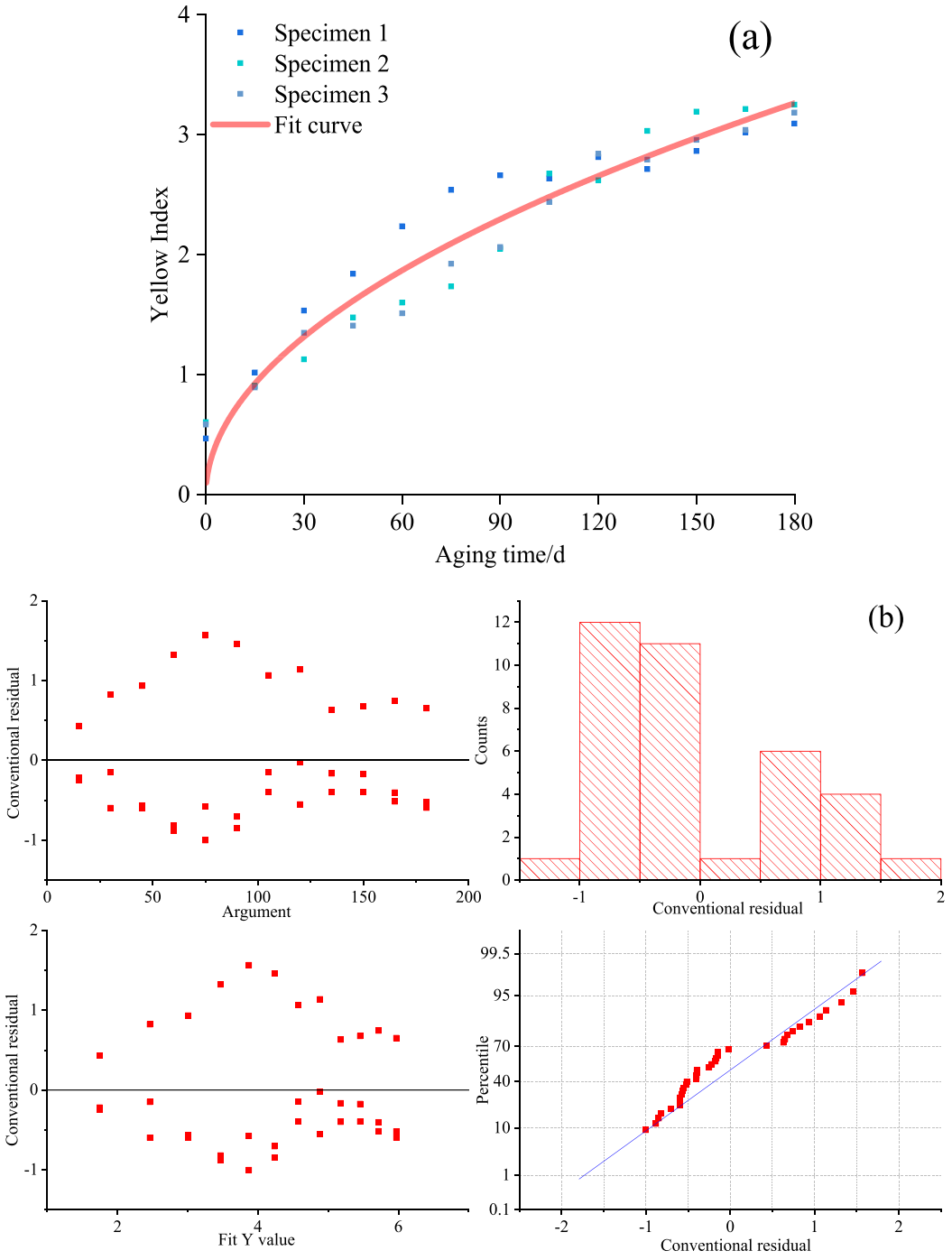

Figure 5. (a) Nonlinear curve fitting. (b) Nonlinear curve fitting residual plot.

data to better capture the abstract features of the data. It can learn and store a large number of input-output pattern mappings without revealing the mathematical equations that describe these mappings beforehand. Its learning rule uses the steepest descent method to continuously adjust the network's weights and thresholds through BP to minimize the sum of squared errors. The topology of the BPNN model includes an input layer, a hidden layer, and an output layer.

As shown in Figure 6, the BPNN model was constructed by using MATLAB software in this study.

4.2.1. Variable Selection. The sample uses the yellowing index test results of PMMA with different aging times in the experiment. The experimental data from 0 to 120 days are used as training samples, and the experimental data from 120 to 180 days are used as testing samples. The input variable is aging time, and the output variable is the yellowing index.

4.2.2. Model Construction. The literature has proved that a three-layer BPNN can meet the mapping requirements of general functions and can approximate any number of variable functions with any accuracy requirements.[31] The single-hidden-layer BPNN can be used to solve a series of problems such as classification, regression, and pattern recognition, and it can achieve good performance in many tasks. Due to the small-scale data in this study, it may be more appropriate to use a single-hidden-layer network, which is relatively simple and has a faster training speed. Therefore, a three-layer BPNN

https://doi.org/10.1021/acsomega.3c06140
ACS Omega 2023, 8, 47812−47820

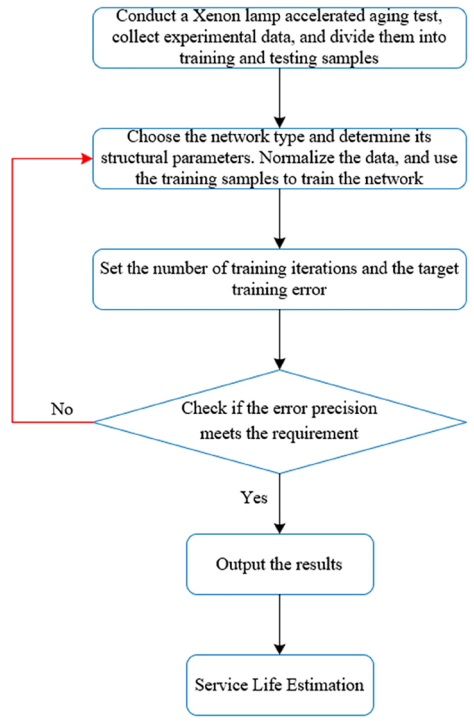

Figure 6. BPNN algorithm flowchart.

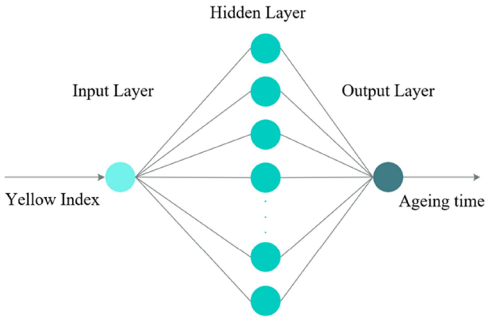

Figure 7. Single-hidden-layer simplified network.

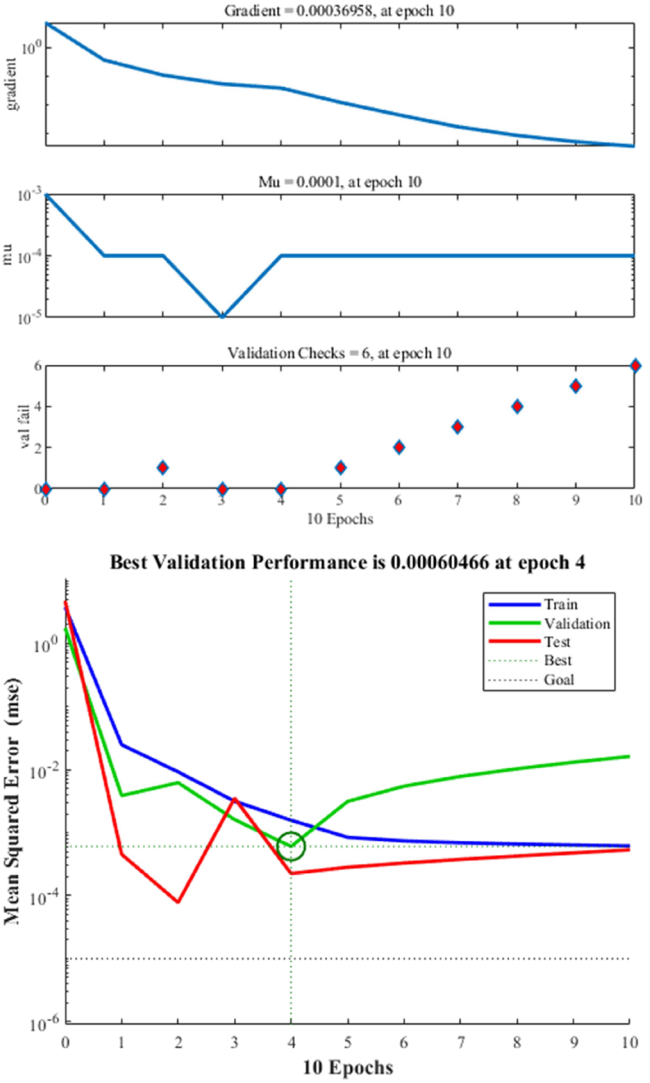

Figure 8. Training state and performance.

is established, which mainly includes the input layer, the output layer, and the hidden layer with the following settings:

Input layer: taking aging time as the input variable, the number of input layer nodes is set to m.

Output layer: taking the yellowing index as the output variable, the number of output layer nodes is set to n.

Hidden layer: the number of hidden layer nodes N is selected using the empirical formula $N = \sqrt{m + n} + a$, where m is the number of input layer nodes, n is the number of output layer nodes, and a is a value between 1 and 10 selected based on the optimal node principle.

The training is carried out using sample vectors with one neuron in the input layer and one neuron in the output layer. Based on the empirical expression for the number of hidden layer neurons and through multiple tests, the optimal number of hidden layer neurons is determined to be 6. The simplified single-hidden-layer network is shown in Figure 7.

4.2.3. Parameter Configuration. In this BPNN, the activation function is the sigmoid function because when the independent variable of this function is greater than a certain value, its function value tends to be 0 or 1, so the initial data need to be normalized. tansig function is used to transfer from the input layer to the hidden layer, and the purelin function is used to transfer from the hidden layer to the output layer. trainlm is used as the training algorithm, and its convergence speed is faster than that of trainbp and trainpx. Generally, the maximum number of iterations is 1000 times, and then, the training convergence is observed. If the convergence is advanced, then the maximum number of iterations is reduced to reach the training goal. The minimum error of the training target is generally 0.001−0.00001, which is adjusted according to the situation of the training test. Too large is easy to overfit, the test effect is poor, and too small can not achieve the desired effect. The learning rate is generally set to 0.01−0.5. The more data there are, the greater the data noise, the more difficult it is to fit the data, and the smaller the value is generally required. If the setting is too large, then it is easy to stop convergence prematurely.

4.2.4. Parameter Optimization. The Grid Search method is used to optimize the training parameters and hyperparameters. It searches the given parameter combination exhaustively, trains and evaluates each combination, and finds the best parameter combination. First, the parameters to be tuned and their range of values. Generate all possible parameter combinations based on the defined parameter space; For

https://doi.org/10.1021/acsomega.3c06140
ACS Omega 2023, 8, 47812−47820

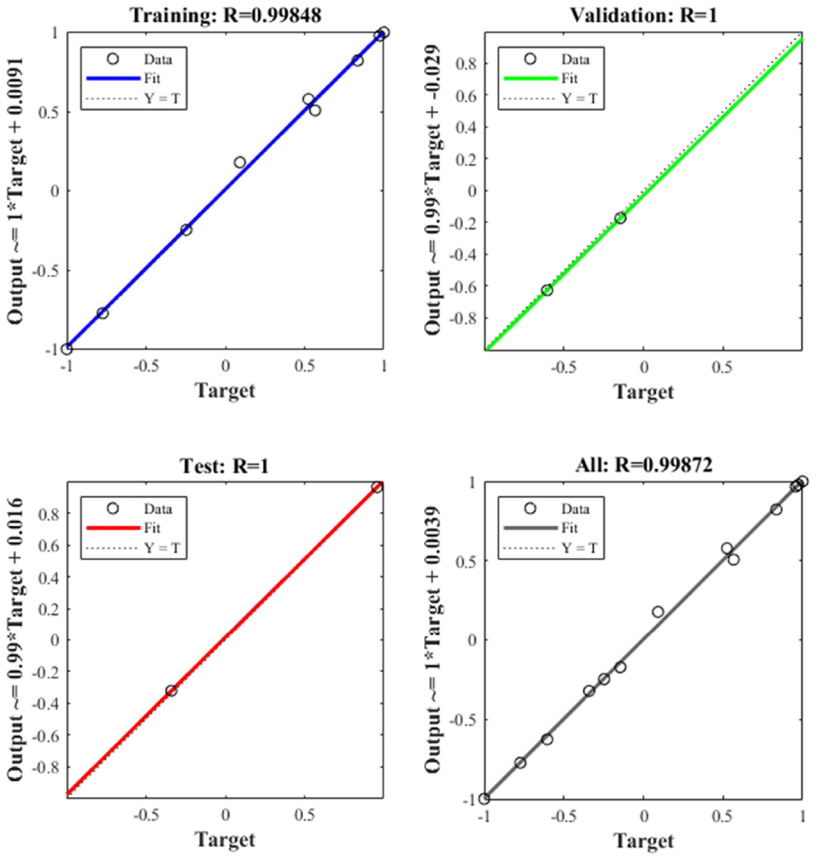

Figure 9. Training, testing, validation, and overall R^2 = 0.9974 were obtained for the training data set.

each parameter combination, use cross-validation or other evaluation methods to evaluate the performance of the model. Finally, according to the evaluation results, the parameter combination with the best performance is selected as the final model parameters.

4.2.5. Training Network. According to the results of parameter optimization, the minimum goal error net.trainparam.goal is set to 0.00001. The learning rate net.trainparam.lr is 0.01; The number of training steps net.trainparam.epochs is 1000. The training process is shown in Figure 8. According to the settings described earlier, the BPNN is trained until it meets the predetermined target, and the training results are shown in Figures 9 and 10. The neural network was iterated 10 times, and the convergence speed was faster and the minimum training error was reached at the fourth iteration.

4.2.6. Model Validation. The simulated Sim function was used to test the trained network using test samples, and the test results were good and were in line with the predetermined settings. The MAE of the model is 0.012479, MSE is 0.019873, and R^2 is 0.97836, which has a good goodness of fit.

4.3. Prediction Results and Discussion. *4.3.1. Initial Data Simulation and Simulation Capability Comparison.* From the above two models, the Goodness of fit of the nonlinear fitting model R^2 is 0.92419, and the MSE is 0.03908; the goodness of fit R^2 of the BPNN model is 0.97836, and the MSE is 0.01987. Among them, the closer R^2 is to 1, the closer MSE is to 0, which means better performance of the model. Compared with the two models, the BPNN model has a higher goodness of fit and better modeling effect.

Comparing the simulated values of the nonlinear fitting model with those of the BPNN model, Table 2 shows that the relative error of the nonlinear fitting model is within ±21%, and the relative error of the BPNN prediction model is within ±12%. Overall, the BPNN model has smaller prediction errors, higher prediction accuracy, and greater stability. However, this does not mean that the BPNN is necessarily the best choice. Other ML models such as random forests (RF), or gradient boosting machines (GBMs) need to be considered. Two gradient boosting methods, in particular, XGBoost and LightGBM, excel in handling tabular data, especially in classification and regression problems. They are both capable of handling large-scale data sets and are fast to train, with high prediction accuracy. These models are also likely to perform well when dealing with tabular data. Therefore, the two algorithms were trained and compared. As shown in Table 3, for both R^2 and MSE, the BP neural network had the best fitting effect, while LightGBM had the worst. The relevant code can be found in Appendix II of the supplementary file.

4.3.2. Life Prediction. Based on the service life of PMMA, the yellow index of the old PMMA sample before aging in this experiment is about 4.5 times that of the new sample. Therefore, this study takes the new PMMA yellow index as the standard to increase 4.5 times, reaching the final service life. Samples 1, 2, and 3 will be withdrawn when the yellow index reaches 2.1028, 2.7217, and 2.6301, respectively. In the BPNN model, the input yellow index is 2.1028, 2.7217, and 2.6301, and the output aging times are 98.3, 126.2, and 123.8 days. Then, the corresponding actual days are A_1, A_2, and A_3.

$$A_1 = 2860.43\ d = 7.83y \tag{8}$$

$$A_2 = 3092.71\ d = 8.47y \tag{9}$$

https://doi.org/10.1021/acsomega.3c06140
ACS Omega 2023, 8, 47812−47820

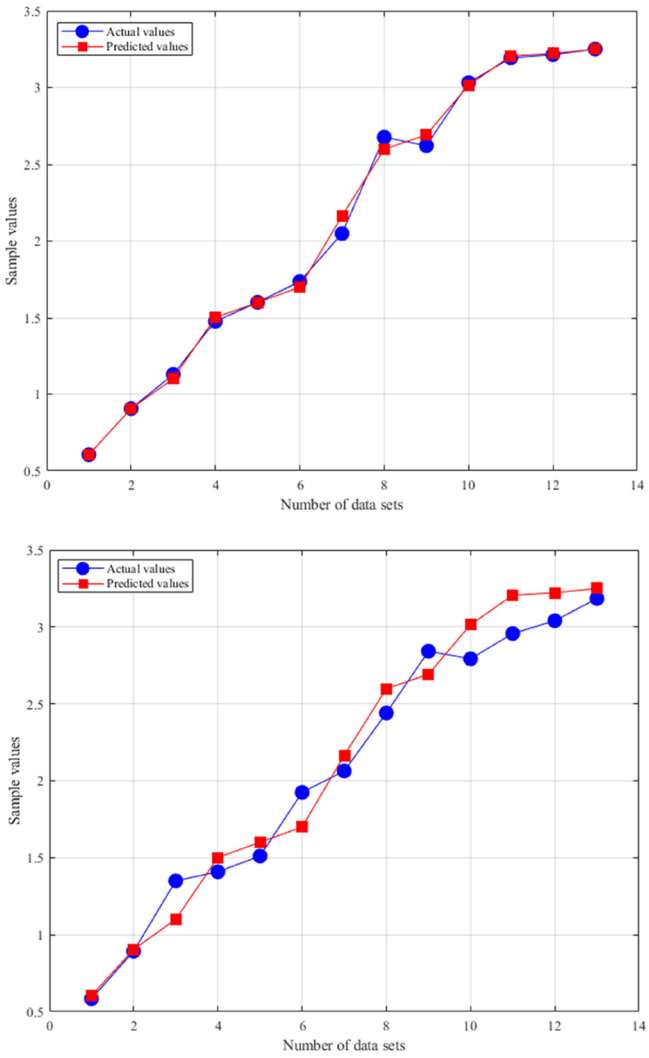

Figure 10. Predicted value vs actual value.

Table 2. Comparison of Actual Values with Simulated Values and Simulated Values

aging time/d	actual value	value of simulation	relative error/%	simulated value	relative error /%
15	0.9028	0.9242	2.3704	0.9043	0.166
30	1.1224	1.3139	17.0617	1.1292	0.6058
45	1.4509	1.6142	11.2551	1.4762	1.7437
60	1.6017	1.8680	16.6261	1.5606	−2.5660
75	1.7377	2.0921	20.3948	1.7399	0.1266
90	2.0411	2.2949	12.4345	2.0401	−0.0490
105	2.6739	2.4817	−7.1880	2.4267	−9.2449
120	2.6202	2.6558	1.3587	2.9337	11.9647
135	3.0304	2.8194	−6.9628	3.0323	0.0627
150	3.1952	2.9743	−6.9135	3.1969	0.0532
165	3.2120	3.1218	−2.8082	3.3366	3.8792
180	3.2524	3.2627	0.3167	3.2528	0.0123

Table 3. Comparison of R^2 and MSE for BPNN, XGBoost, and LightGBM Models

model	R^2	MSE
BPNN	0.97836	0.01987
XGBoost	0.82718	0.12107
LightGBM	0.65045	0.73590

$$A_3 = 3074.21\ d = 8.42y \quad (10)$$

The service life of the three samples is 7.83, 8.47, and 8.42 years, respectively.

5. CONCLUSIONS

(1) A PMMA life prediction modeling strategy was proposed, which obtained experimental data through xenon lamp accelerated aging test using PMMA, and then established a model using BPNN to predict the PMMA life.

(2) In the xenon lamp accelerated aging test, the yellow index of PMMA showed an upward trend with the increase of aging time, and the upward trend gradually became slow; By comparing the yellow index of the old PMMA sample and the new sample after xenon lamp accelerated aging when the accelerated aging time is 105 days, the corresponding natural aging time is 8 years, then the aging factor at the aging temperature of 55 °C and the actual temperature of 23 °C is 681.96.

(3) The life prediction model of PMMA is established by using nonlinear curve fitting and BPNN. By comparing their goodness of fit, mean squared error, and simulation ability, the BPNN has higher prediction accuracy than nonlinear curve fitting. Taking the yellow index of PMMA after eight years of use as the standard, the life of three samples of newly produced PMMA is calculated as 7.83, 8.47, and 8.42 years, respectively, through the output data of the BPNN prediction model. The performance and exhibition effects of PMMA are poor, and a batch of organic glass needs to be updated.

■ ASSOCIATED CONTENT

Supporting Information

The Supporting Information is available free of charge at https://pubs.acs.org/doi/10.1021/acsomega.3c06140.

Appendix I summarizes the *X*, *Y*, and *Z* data used to calculate the yellow index by the colorimeter test; Appendix II summarizes the BP neural network code used through MATLAB 2019b (PDF)

■ AUTHOR INFORMATION

Corresponding Authors

Xuegang Liu − *Jingzhou Conservation Center, Jingzhou 434020, China*; Email: liuxuegang705@163.com

Yang Lei − *School of Chemistry and Chemical Engineering, Hubei Key Laboratory of Coal Conversion and New Carbon Materials, Wuhan University of Science and Technology, Wuhan 430081, China*; orcid.org/0000-0002-1975-3569; Email: leiyang@wust.edu.cn

Authors

Yang Zhang − *School of History and Culture, Hubei University, Wuhan 430062, China; School of Chemistry and Chemical Engineering, Hubei Key Laboratory of Coal Conversion and New Carbon Materials, Wuhan University of Science and Technology, Wuhan 430081, China; Jingzhou Conservation Center, Jingzhou 434020, China*

Ke Wang − *School of Chemistry and Chemical Engineering, Hubei Key Laboratory of Coal Conversion and New Carbon Materials, Wuhan University of Science and Technology,*

https://doi.org/10.1021/acsomega.3c06140
ACS Omega 2023, 8, 47812−47820

Wuhan 430081, China; orcid.org/0009-0005-6258-1984

Hao Peng − *Jingzhou Museum, Jingzhou 434020, China*

Yanfen Huang − *School of Chemistry and Chemical Engineering, Hubei Key Laboratory of Coal Conversion and New Carbon Materials, Wuhan University of Science and Technology, Wuhan 430081, China;* orcid.org/0000-0002-4835-8314

Hai An − *Shanxi Academy of Ancient Building and Painted Sculpture & Fresesco Preservation, Taiyuan 030012, China*

Complete contact information is available at: https://pubs.acs.org/10.1021/acsomega.3c06140

Notes

The authors declare no competing financial interest.

■ ACKNOWLEDGMENTS

The authors gratefully acknowledge the financial support from the Open Project of Key Scientific Research Base of the National Cultural Heritage Administration for the Protection of Unearthed Wood Lacquerware (2021H10198).

■ REFERENCES

(1) Kowalonek, J.; Kaczmarek, H.; Kurzawa, M. Effect of UV-irradiation on fluorescence of poly (methyl methacrylate) films with photosensitive organic compounds. *J. Photochem. Photobiol., A* **2016**, *319*, 18−24.

(2) Münker, T.; Van de Vijfeijken, S.; Mulder, C. S.; et al. Effects of sterilization on the mechanical properties of poly (methyl methacrylate) based personalized medical devices. *Journal of The Mechanical Behavior of Biomedical Materials* **2018**, *81*, 168−172.

(3) Zhong, Z. W.; Wang, Z. F.; Zirajutheen, B. M. P. Chemical mechanical polishing of polycarbonate and poly methyl methacrylate substrates. *Microelectron. Eng.* **2005**, *81* (1), 117−124.

(4) Manjunatha, H. C. A study of gamma attenuation parameters in poly methyl methacrylate and Kapton. *Radiat. Phys. Chem.* **2017**, *137*, 254−259.

(5) Ali, U.; Karim, K. J. B. A.; Buang, N. A. A review of the properties and applications of poly (methyl methacrylate)(PMMA). *Polym. Rev.* **2015**, *55* (4), 678−705.

(6) Bussi, Y.; Golan, S.; Dosoretz, C. G.; et al. Synthesis, characterization, and performance of polystyrene/PMMA blend membranes for potential water treatment. *Desalination* **2018**, *431*, 35−46.

(7) Deka, N.; Bera, A.; Roy, D.; et al. Methyl methacrylate-based copolymers: recent developments in the areas of transparent and stretchable active matrices. *ACS Omega* **2022**, *7* (42), 36929−36944.

(8) Khoshaim, A. B.; Elsheikh, A. H.; Moustafa, E. B.; et al. Prediction of residual stresses in turning of pure iron using artificial intelligence-based methods. *Journal of Materials Research and Technology* **2021**, *11*, 2181−2194.

(9) Nasiri, S.; Khosravani, M. R. Machine learning in predicting mechanical behavior of additively manufactured parts. *Journal of Materials Research and Technology* **2021**, *14*, 1137−1153.

(10) Liu, X.; Mutailipu, M.; Zhao, J.; et al. Comparative analysis of four neural network models on the estimation of CO_2−brine interfacial tension. *ACS Omega* **2021**, *6* (6), 4282−4288.

(11) Elsheikh, A. H.; Muthuramalingam, T.; Shanmugan, S.; et al. Fine-tuned artificial intelligence model using pigeon optimizer for prediction of residual stresses during turning of Inconel 718. *Journal of Materials Research and Technology* **2021**, *15*, 3622−3634.

(12) Yin, W.; Xie, Z.; Yin, Y.; et al. Aging behavior and lifetime prediction of PMMA under tensile stress and liquid scintillator conditions. *Advanced Industrial and Engineering Polymer Research* **2019**, *2* (2), 82−87.

(13) Murray, M. P.; Bruckman, L. S.; French, R. H. Photodegradation in a stress and response framework: poly (methyl methacrylate) for solar mirrors and lens. *J. Photon. Energy* **2012**, *2* (1), No. 022004.

(14) Yousif, E.; Haddad, R. Photodegradation and photostabilization of polymers, especially polystyrene: review. *SpringerPlus* **2013**, *2* (1), 398.

(15) Miller, D. C.; Carloni, J. D.; Johnson, D. K.; et al. An investigation of the changes in poly (methyl methacrylate) specimens after exposure to ultra-violet light, heat, and humidity. *Sol. Energy Mater. Sol. Cells* **2013**, *111*, 165−180.

(16) de Castro Monsores, K. G.; da Silva, A. O.; de Sant' Ana Oliveira, S.; Rodrigues, J. G. P.; Weber, R. P. Influence of ultraviolet radiation on polymethylmethacrylate (PMMA). *J. Mater. Res. Technol.* **2019**, *8* (5), 3713−3718.

(17) Kechagias, J. D.; Ninikas, K.; Stavropoulos, P.; et al. A generalised approach on kerf geometry prediction during CO_2 laser cut of PMMA thin plates using neural networks. *Lasers in Manufacturing and Materials Processing* **2021**, *8* (3), 372−393.

(18) Kuo, C. F. J.; Tsai, W. L.; Su, T. L.; Chen, J. L. Application of an LM-neural network for establishing a prediction system of quality characteristics for the LGP manufactured by CO_2 laser. *Opt. Laser Technol.* **2011**, *43* (3), 529−536.

(19) Chen, X.; Sztandera, L.; Cartwright, H. M. A neural network approach to prediction of glass transition temperature of polymers. *International Journal of Intelligent Systems* **2008**, *23* (1), 22−32.

(20) Asante-Okyere, S.; Xu, Q.; Mensah, R. A.; et al. Generalized regression and feed forward back propagation neural networks in modelling flammability characteristics of polymethyl methacrylate (PMMA). *Thermochim. Acta* **2018**, *667*, 79−92.

(21) Khanlou, H. M.; Sadollah, A.; Ang, B. C.; et al. Prediction and optimization of electrospinning parameters for polymethyl methacrylate nanofiber fabrication using response surface methodology and artificial neural networks. *Neural Computing and Applications* **2014**, *25*, 767−777.

(22) Kimmig, J.; Schuett, T.; Vollrath, A.; Zechel, S.; Schubert, U. S. Prediction of nanoparticle sizes for arbitrary methacrylates using artificial neuronal networks. *Adv. Sci.* **2021**, *8* (23), No. 2102429.

(23) D'Addona, D. M.; Genna, S.; Leone, C.; et al. Prediction of poly-methyl-methacrylate laser milling process characteristics based on neural networks and fuzzy data. *Procedia Cirp* **2016**, *41*, 981−986.

(24) Wiangkham, A.; Ariyarit, A.; Aengchuan, P. Prediction of the mixed mode I/II fracture toughness of PMMA by an artificial intelligence approach. *Theoretical and Applied Fracture Mechanics* **2021**, *112*, 102910−102920.

(25) Paturi, U. M. R.; Kolluru, S. K. P.; Kalvakolanu, S. D. S. A. Prediction of weld-line width and sink-mark depth of plastic injection moulded parts using neural networks. *Mater. Today: Proc.* **2023**, 1−10.

(26) Chen, K.; Zhang, T.; Bao, S. Water absorption rate prediction of PMMA and its composites using BP neural network[C]. MATEC Web of Conferences. *EDP Sciences* **2016**, *67*, 06017−06024.

(27) Sadan, M. K.; Ahn, H. J.; Chauhan, G. S.; et al. Quantitative estimation of poly (methyl methacrylate) nano-fiber membrane diameter by artificial neural networks. *Eur. Polym. J.* **2016**, *74*, 91−100.

(28) Youzhuang, S.; Junhua, Z.; Yongan, Z. Echo state neural network based on an improved gray wolf algorithm predicts porosity through logging data. *ACS Omega* **2023**, *8*, 21182−21194.

(29) Motulsky, H. J.; Ransnas, L. A. Fitting curves to data using nonlinear regression: a practical and nonmathematical review. *FASEB J.* **1987**, *1* (5), 365−374.

(30) Gavin, H P. *The Levenberg-Marquardt algorithm for nonlinear least squares curve-fitting problems*; Department of Civil and Environmental Engineering, Duke University, 2019; pp 1−19.

(31) Buscema, M. Back propagation neural networks. *Substance use & misuse* **1998**, *33* (2), 233−270.